J. Am. Ceram. Soc., 1–5 (2016)
DOI: 10.1111/jace.14276

journal

Fabrication and Microwave Dielectric Properties of Mg_2SiO_4-$LiMgPO_4$-TiO_2 Composite Ceramics

ZiFan Cheng, Xing Hu,† Yi Li, and ZhiYuan Ling

Department of Electronic Materials Science and Engineering, South China University of Technology, Guangzhou 510640, China

Complete solid solutions between Mg_2SiO_4 and $LiMgPO_4$ are confirmed by the XRD results. The phase constitution of $0.5Mg_2SiO_4$-$0.5LiMgPO_4$ is found to be dependent on firing temperature. The chemical compatibility between Mg_2SiO_4 and rutile phase at sintering temperature is modified by incorporating $LiMgPO_4$. The microwave dielectric properties of $(1-y)(0.5Mg_2SiO_4$-$0.5LiMgPO_4)$-$yTiO_2$ (y = 0–0.3) composite ceramics have been investigated. The optimized microwave dielectric properties for $0.35Mg_2SiO_4$-$0.35LiMgPO_4$-$0.3TiO_2$ ceramics sintered at 1050°C show low dielectric constant (11.4), high-quality factor (31 800 GHz), and low-temperature coefficient of resonant frequency (−4 ppm/°C).

Keywords: *microwave dielectrics; forsterite; $LiMgPO_4$*

I. Introduction

Recently, much attention has been paid to the development of microwave telecommunication technologies because of the increased requirements for microwave applications. These applications demand microwave substrate materials with high-quality factor ($Q \times f$) to achieve high selectivity, low dielectric constant (ε_r) to reduce the delay time of electronic signal transmission, and almost zero temperature coefficient of resonant frequency (τ_f) for frequency stability. In the past years, a large number of ceramics with good microwave dielectric properties have been reported as promising candidates for substrate application, such as Mg_2SiO_4 ($Q \times f$ = 240 000 GHz, ε_r = 6–7, τ_f = −60 ppm/°C),[1] Al_2O_3 ($\tan\delta = 2.7 \times 10^{-5}$ at 10 GHz, ε_r = 10),[2] MgO (ε_r = 7–10, $Q \times f$ = 113 600 GHz),[3,4] and Li_2MgSiO_4 ($\tan\delta = 5.2 \times 10^{-4}$ at 8 GHz, ε_r = 5.1).[5] Among these materials, forsterite Mg_2SiO_4 has attracted a great attention with low dielectric constant and high-quality factor.[6–10]

Forsterite Mg_2SiO_4 is mainly composed of the anion SiO_4^{4-} and the cation Mg^{2+} in a molar ratio 1:2. It is expected for forsterite to have low dielectric constant because of silica-oxygen tetrahedra composed of half covalent bonds.[11,12] Although forsterite ceramic is suggested to be candidate for microwave substrate material, several issues should be addressed, such as high sintering temperature (1400°C), the large negative τ_f (−60 to −70 ppm/°C), and existence of a second phase.[13] To reduce densification temperature of ceramics, researchers reported several methods using low melting oxide or glass additions such as B_2O_3, CuO, CaO-B_2O_3-SiO_2, V_2O_5, and Li_2CO_3, etc.[14–16] To adjust the temperature coefficient of resonant frequency, some additions with large positive τ_f such as TiO_2 (ε_r ~90, $Q \times f$ = 113 600 GHz, τ_f = +450 ppm/°C)[17] were doped in the ceramics. However, Mg_2SiO_4 reacted with TiO_2 at the high sintering temperature and the formation of secondary phases such as $MgSiO_3$, $MgTi_2O_5$, and $MgTiO_3$ caused the decrease in $Q \times f$ value and increase in dielectric constant. To prevent the production of the secondary phase, liquid phase deposition method was performed by adding TiO_2 into porous Mg_2SiO_4,[6] but the mechanical strength of ceramics was greatly reduced.

Recently, the $LiMgPO_4$ ceramic with olivine-type structure[18] was reported to have good microwave properties of ε_r = 6.6 and $Q \times f$ = 79 100 GHz.[19] Although the $LiMgPO_4$ has the same structure with Mg_2SiO_4, it has been found to have a good chemical compatibility with TiO_2 at sintering temperature.[19] It is interesting to tune the chemical compatibility between Mg_2SiO_4 and TiO_2 by incorporating $LiMgPO_4$. In this paper, solid solutions of Mg_2SiO_4-$LiMgPO_4$ were investigated together with their chemical compatibilities with rutile phase. Microwave dielectric properties were also investigated for ceramics of $(1-y)$[$0.5Mg_2SiO_4$-$0.5LiMgPO_4$]-$yTiO_2$ (y = 0-0.3).

II. Experimental Procedure

High-purity powders (≥99.9%) of Li_2CO_3, MgO, SiO_2, TiO_2 (rutile), and ammonium polyphosphate [$(NH_4)_{n+2}P_nO_{3n+1}$, APP) were used as the starting materials, weighed in a stoichiometric ratio and ball milled in ethanol with zirconia balls for 1.5 h. Mg_2SiO_4-$LiMgPO_4$ powders were synthesized using the conventional solid-state reaction method by calcining in an alumina crucible in the range 750°C–1200°C for 3 h. Those calcined powders were ground into fine powders and remilled with the same condition in previous process. The chemical compatibility of Mg_2SiO_4-$LiMgPO_4$ and rutile phase was performed by mixing and homogenizing powdered TiO_2 with the calcined powder and firing at a temperature 950°C–1200°C for 3 h to achieve equilibrium. According to the desired stoichiometry $(1-y)$[$0.5Mg_2SiO_4$-$0.5LiMgPO_4$]-$yTiO_2$ (y = 0–0.3), the dried powders, with 6 wt% PVA (polyvinyl alcohol) added, were pressed into rods of 10 mm diameter and 5 mm thickness under a pressure of 20 000 psi and these compacts were sintered at temperatures from 1025°C to 1150°C in air for 3 h.

Phase constitutions were identified by X-ray diffraction (XRD) patterns using Cu$K\alpha$ radiation (Rigaku D/max-IIIA, Tokyo, Japan). The step-scan mode was used with setup of 40 kV × 40 mA, step 0.01°, 0.2 s per step.[20] Rietveld refinement was conducted using FullProf Suite program. The bulk densities of the sintered bodies were determined by the Archimedes method. The morphologies of the polished ceramics were examined with an ZEISS EVO 18 tungsten wire filament scanning electron microscope and the EDS analysis was also performed (Carl Zeiss Jena, Oberkochen, Germany). The microwave dielectric properties were evaluated by Hakki and Coleman's resonator method (Agilent E8363B network analyzer, Santa Clara, CA). The temperature coefficient of resonant frequency (τ_f) was estimated from the Eq. (1) where α is the linear expansion coefficient ($\alpha \approx 10$ ppm/°C), and τ_ε is the

N. Alford—contributing editor

Manuscript No. 37527. Received September 18, 2015; approved March 28, 2016.
†Author to whom correspondence should be addressed. e-mail: huxing@scut.edu.cn

temperature coefficient of dielectric constant evaluated at 1 MHz by an LCR meter (HP 4288A; Agilent) equipped with a thermostat range from 25°C to 85°C.[21]

$$\tau_f(\text{ppm}/^\circ\text{C}) = -\left(\alpha + \frac{1}{2}\tau_\varepsilon\right) \quad (1)$$

III. Results and Discussion

The crystal structure of forsterite Mg_2SiO_4 with A_2BO_4 formula can be described as a hexagonal, close-packed array of oxygen ions with one-half of the octahedral sites occupied by Mg^{2+} cation in A-site and one-eighth of the tetrahedral sites occupied by Si^{4+}, which is in B-site.[11] Considering that the ion radius of Li^+ (0.76 Å) is similar with that of Mg^{2+} (0.72 Å) and the ion radius of P^{5+} (0.17 Å) is similar with that of Si^{4+} (0.26 Å),[22] Mg^{2+} could be replaced by Li^+ and Si^{4+} could be replaced by P^{5+}. The charge balance is also obtained by replacing ($Mg^{2+}Si^{4+}$) with (Li^+P^{5+}). The solid solution phases between Mg_2SiO_4 and $LiMgPO_4$ are determined by the XRD patterns of Fig. 1. The peaks in Fig. 1 can be well indexed using standard JCPDS files (file No: #85-1364 for Mg_2SiO_4 and #32-0574 for $LiMgPO_4$), and the diffraction patterns are attributed to orthorhombic structure with space group *Pbnm*. Magnified XRD patterns of $(1-x)Mg_2SiO_4$-$xLiMgPO_4$ ceramics are shown in Fig. 2(a). The diffraction peak of [130] moves to higher angle with the increasing content of $LiMgPO_4$ and it reveals that the related lattice parameters decrease. The lattice parameters are determined by the Rietveld refinement method, and the cell volume decreases with the increasing content of $LiMgPO_4$ as shown in Fig. 2(b) and Table I. The Rietveld refinement and the microstructure analysis of $0.5Mg_2SiO_4$-$0.5LiMgPO_4$ ceramic are also given in Fig. 3. The backscattered electron image shows the single phase for the composition and the EDS results confirms the coexistence of Mg, Si, and P.

Both the above results of EDS and XRD patterns show the complete solid solution could be obtained when substituting (LiP) for (MgSi) in Mg_2SiO_4. However, comparing with the sample fired at 1150°C, the composition of $0.5Mg_2SiO_4$-$0.5LiMgPO_4$ calcined at 900°C shows the different crystal chemistry. As shown in Fig. 4(a), the splitting of diffraction peaks is observed for the sample calcined at 900°C and it is attributed to the coexistence of Mg_2SiO_4-rich phase and $LiMgPO_4$-rich phase. The splitting of diffraction peaks disappears when the firing temperature increases to 1150°C [Fig. 4(b)] and the solid solution of $(Mg_{0.75}Li_{0.25})(Si_{0.5}P_{0.5})O_4$ is obtained.

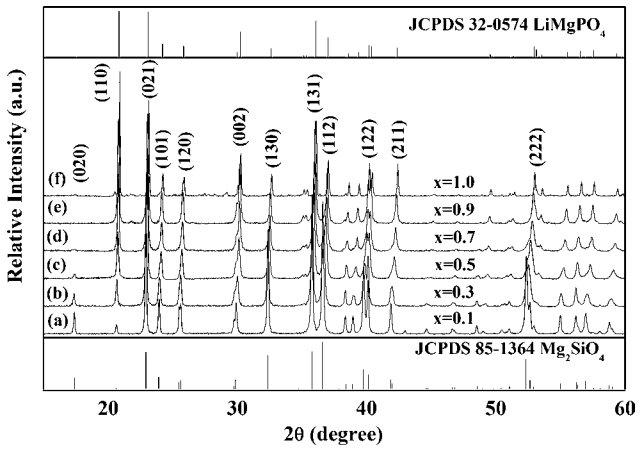

Fig. 1. XRD patterns of $(1-x)Mg_2SiO_4$-$xLiMgPO_4$ ceramics fired at different temperature: (a) $x = 0.1$ at 1200°C, (b) $x = 0.3$ at 1200°C, (c) $x = 0.5$ at 1150°C, (d) $x = 0.7$ at 1100°C, (e) $x = 0.9$ at 1000°C, and (f) $x = 1.0$ at 950°C.

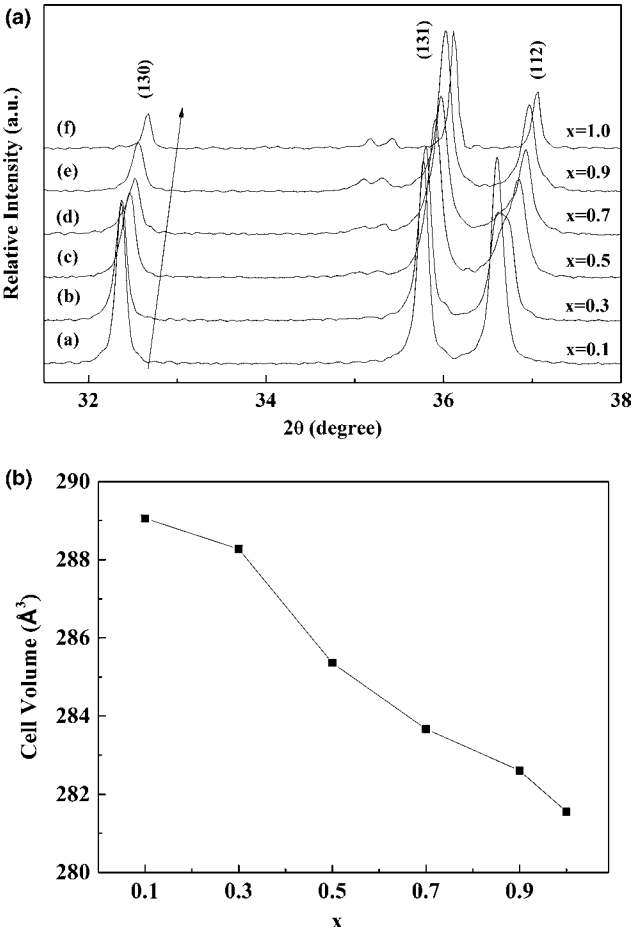

Fig. 2. (a) Magnified XRD patterns of $(1-x)Mg_2SiO_4$-$xLiMgPO_4$ ceramics in the range 32°–38°; (b) the cell volume of $(1-x)Mg_2SiO_4$-$xLiMgPO_4$ ceramics.

Both Mg_2SiO_4 and $LiMgPO_4$ have a negative temperature coefficient of τ_f, so rutile phase of TiO_2 with a positive τ_f can be incorporated to adjust τ_f of the solid solution of Mg_2SiO_4-$LiMgPO_4$ to near zero. The chemical compatibilities at sintering temperature between $(1-x)Mg_2SiO_4$-$xLiMgPO_4$ and TiO_2 are investigated by the XRD patterns as shown in Fig. 5. When $x = 0.1$ and 0.3, $MgTi_2O_5$ (JCPDS files No: #79-0832) is observed and only trace of TiO_2 is observed at $x = 0.1$. As mentioned by Tsunooka et al.,[1] $MgTi_2O_5$ phase was created in the reaction between Mg_2SiO_4 and TiO_2 and TiO_2 does not exist as a single phase until over 50 wt% according to the MgO-SiO_2-TiO_2 ternary phase diagram. When $x = 0.5$, 0.7 and 0.9, solid solution of forsterite phase is chemical compatible to the rutile phase. When $x = 1$, $LiTiPO_5$ (JCPDS files No: #77-0789) is observed as a secondary phase and it is very different from the result of Thomas et al.[19]

As mentioned above, Mg_2SiO_4 will react with TiO_2 at high temperature to form $MgTi_2O_5$. It means the Mg–O bond is easy to be broken and Mg is released to react with TiO_2. Average bond length could be used to evaluate the resistance to disruption of oxygen polyhedra in crystal structures.[23] Considering the cell volume of Mg_2SiO_4 and $LiMgPO_4$ [Fig. 2(b)], the average bond strength of A–O in $LiMgPO_4$ will be higher than that in Mg_2SiO_4 because of the shorter average bond length of A–O in $LiMgPO_4$. For $LiMgPO_4$, the larger LiO_6 octahedron with larger ion radius of Li^+ will compress the MgO_6 octahedron and it can also strengthen the Mg-O bond. In $LiMgPO_4$, the average bond distance of Li (M1 site)-O and Mg (M2 site)-O is 2.1427 Å and 2.1053 Å, respectively.[18] In Mg_2SiO_4, the average bond distance of Mg1 (M1 site)-O and Mg2 (M2 site)-O is 2.0942

Table I. Crystal Lattice Parameters of $(1-x)Mg_2SiO_4$-$xLiMgPO_4$

x	a (Å)	b (Å)	c (Å)	Cell volume (Å^3)	R_p (%)	R_{wp} (%)	R_{exp} (%)
0.1	4.7460(5)	10.2007(6)	5.9706(1)	289.05(7)	10.6	9.94	8.41
0.3	4.7391(6)	10.2068(3)	5.9595(2)	288.27(3)	13.4	13.0	8.56
0.5	4.7212(3)	10.1874(1)	5.9329(8)	285.35(9)	12.7	14.3	8.40
0.7	4.7073(1)	10.1753(7)	5.9222(6)	283.66(8)	17.2	14.8	9.45
0.9	4.7014(8)	10.1617(6)	5.9153(0)	282.60(5)	13.1	13.7	9.33
1	4.6950(5)	10.1491(1)	5.9086(9)	281.55(2)	17.9	17.8	9.22

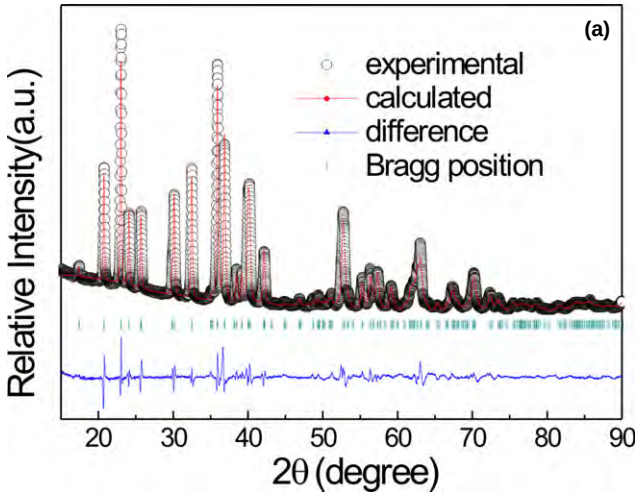

Fig. 3. (a) Rietveld refinements; (b) backscattered scanning electron micrograph and EDS analysis of the $0.5Mg_2SiO_4$-$0.5LiMgPO_4$ ceramics.

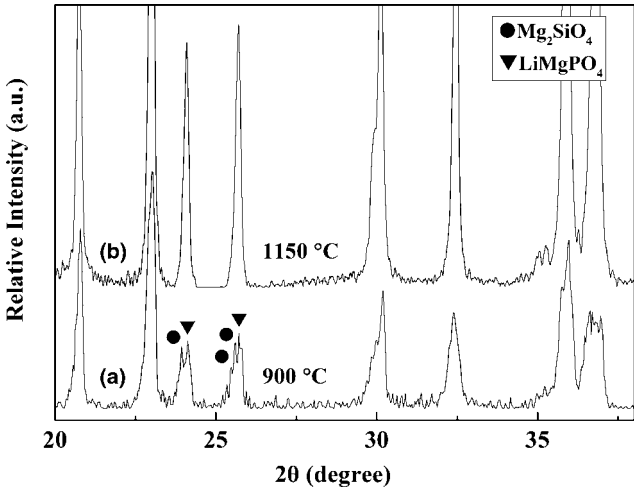

Fig. 4. XRD patterns of $0.5Mg_2SiO_4$-$0.5LiMgPO_4$ ceramics fired at (a) 900°C; (b) 1150°C.

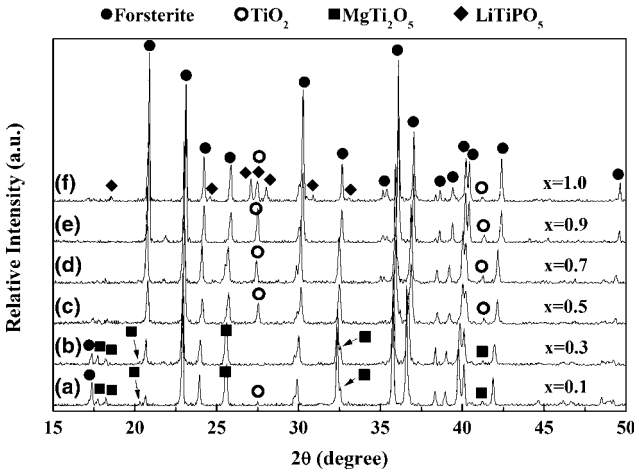

Fig. 5. XRD patterns of $0.9[(1-x)Mg_2SiO_4$-$xLiMgPO_4]$–$0.1TiO_2$ ceramics: (a) $x = 0.1$, (b) $x = 0.3$, (c) $x = 0.5$, (d) $x = 0.7$, (e) $x = 0.9$, and (f) $x = 1.0$ fired at 950°C–1200°C for 3 h in air.

and 2.1287 Å, respectively.[24] The different bond distance and bond strength of Mg (M2 site)-O contributes to the difference crystal chemistry between $LiMgPO_4$ and Mg_2SiO_4. When incorporating $LiMgPO_4$ into Mg_2SiO_4, the solid solution for $x \geq 0.5$ has good chemical compatibility with TiO_2 due to the improved Mg–O bond strength.

Because the reported $Q \times f$ value of Mg_2SiO_4 is higher than that of $LiMgPO_4$,[1,19] the composition of $x = 0.5$ is selected in further research considering it more close to Mg_2SiO_4 together with the chemical compatibility with rutile. To make the temperature coefficient of resonant frequency adjustable, $0.5Mg_2SiO_4$-$0.5LiMgPO_4$ should be chemical compatible with various content of rutile. XRD patterns of $(1-y)[0.5Mg_2SiO_4$-$0.5LiMgPO_4]$-$yTiO_2$ ($y = 0$–0.3) ceramics are shown in Fig. 6 and the results reveal only TiO_2 phase and forsterite phase are found. So, it is possible to develop a composition with τ_f near zero by incorporating rutile into $0.5Mg_2SiO_4$-$0.5LiMgPO_4$.

The densities of $(1-y)[0.5Mg_2SiO_4$-$0.5LiMgPO_4]$-$yTiO_2$ ceramics sintered at different temperature are shown in Fig. 7. When $y = 0$, the maximum of density is obtained at 1150°C which is quite lower than the sintering temperature for densified Mg_2SiO_4 ceramic. It is found that the addition of rutile phase can decrease the sintering temperature of $0.5Mg_2SiO_4$-$0.5LiMgPO_4$ ceramics from 1150°C to 1050°C–1100°C. When $y = 0.2$–0.3, the stable densities for ceramics sintered at 1050°C–1125°C reveal the widened sintering temperature window.

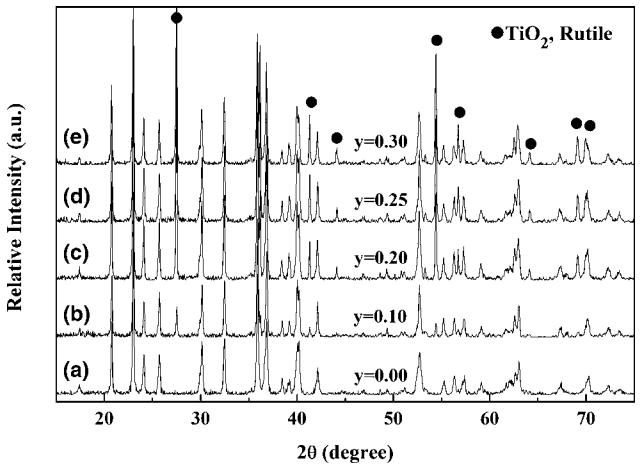

Fig. 6. XRD patterns of $(1-y)[0.5Mg_2SiO_4\text{-}0.5LiMgPO_4]$–$yTiO_2$ ceramics (a) $y = 0.00$, (b) $y = 0.10$, (c) $y = 0.20$, (d) $y = 0.25$, and (e) $y = 0.30$ sintered at 1050°C–1150°C for 3 h in air.

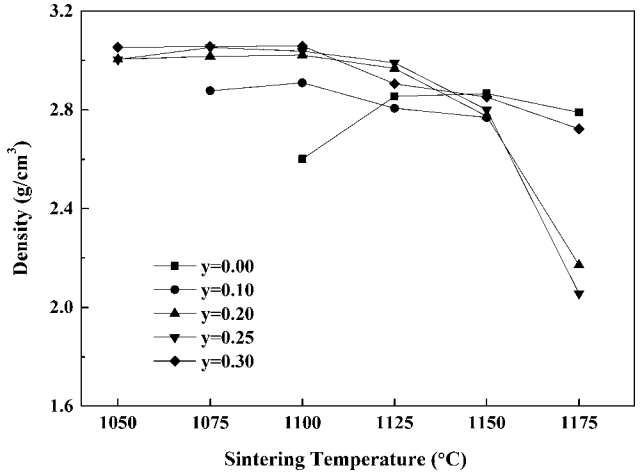

Fig. 7. Density versus sintering temperature of $(1-y)[0.5Mg_2SiO_4\text{-}0.5LiMgPO_4]$–$yTiO_2$ ($y = 0.00, 0.10, 0.20, 0.25, 0.30$) ceramics.

Microwave dielectric properties of $(1-y)[0.5Mg_2SiO_4\text{-}0.5LiMgPO_4]\text{-}yTiO_2$ ceramics were shown in Table II. With the increasing rutile content, the dielectric constant of ceramics increases from 6.7 to 11.4 and the temperature coefficient resonant frequency reduced from −79 to −4 ppm/°C. The highest $Q \times f$ value is obtained for the ceramics without rutile addition. The sintering temperature has also an influence on the microwave dielectric properties such as for $y = 0.3$. The optimized microwave properties were obtained for the composition of $y = 0.3$ sintered at 1050°C such as low τ_f (−4 ppm/°C), high value of $Q \times f$ (31 800 GHz) and low dielectric constant (11.4). For the composition of $y = 0.3$, the calculated volume fraction of TiO_2 (0.16) is slightly higher than the volume fraction of TiO_2 (0.12) in $LiMgPO_4$-TiO_2 to get near zero τ_f.[19]

Table II. Microwave Dielectric Properties of $(1-y)(0.5Mg_2SiO_4\text{-}0.5LiMgPO_4)\text{-}yTiO_2$ ($y = 0.00$–0.30)

y	Sintering temperature (°C)	ε_r	Q × f (GHz)	τ_f (ppm/°C)
0.00	1150	6.7	39 900	−79
0.10	1100	7.8	18 400	−79
0.20	1100	8.9	34 400	−39
0.25	1100	10.1	32 700	−24
0.30	1050	11.4	31 800	−4
0.30	1100	11.1	25 900	−2

IV. Conclusion

In present work, Mg_2SiO_4-$LiMgPO_4$-TiO_2 composite ceramics were fabricated by solid-state reaction method. The solid solutions of $(1-x)Mg_2SiO_4\text{-}xLiMgPO_4$ ($x = 0.1$–0.9) are confirmed by the XRD patterns. The coexistence of Mg_2SiO_4-rich phase and $LiMgPO_4$-rich phase for $0.5Mg_2SiO_4\text{-}0.5LiMgPO_4$ calcined at 900°C shows the temperature dependence of the phase constitution. The compatibility test between $(1-x)Mg_2SiO_4\text{-}xLiMgPO_4$ and TiO_2 shows the solid solution for $x \geq 0.5$ has good chemical compatibility with TiO_2 due to the improved Mg–O bond strength. The optimized microwave dielectric ceramics sintered 1050°C for composition of $0.35Mg_2SiO_4\text{-}0.35LiMgPO_4\text{–}0.3TiO_2$ shows low dielectric constant (11.4), high-quality factor (31 800 GHz), and low-temperature coefficient of resonant frequency (−4 ppm/°C).

Acknowledgments

This work was supported by Guangzhou Nova Program (2012J2200013).

Reference

[1]T. Tsunooka, M. Androu, Y. Higashida, H. Sugiurab, and H. Ohsatoc, "Effects of TiO_2 on Sinterability and Dielectric Properties of High-Q Forsterite Ceramics," *J. Eur. Ceram. Soc.*, **23** [14] 2573–8 (2003).

[2]N. M. Alford and S. J. Penn, "Sintered Alumina with Low Dielectric Loss," *J. Appl. Phys.*, **80** [10] 5895–8 (1996).

[3]J. Y. Chen, W. H. Hsu, and C. L. Huang, "Dielectric Properties of Magnesium Oxide at Microwave Frequency," *J. Alloy. Compd.*, **504** [1] 284–7 (2010).

[4]L. J. Tang, J. W. Wang, J. Zhai, J. W. Zhai, L. B. Kong, and X. Yao, "Controllable-Permittivity and High-Tunability of $Ba_{0.5}Sr_{0.5}TiO_3$/MgO Based Ceramics by Composite Configuration," *Appl. Phys. Lett.*, **102** [14] 142907 (2013).

[5]S. George, P. S. Anjana, V. N. Deepu, P. Mohanan, and M. T. Sebastian, "Low-Temperature Sintering and Microwave Dielectric Properties of Li_2MgSiO_4 Ceramics," *J. Am. Ceram. Soc.*, **92** [6] 1244–9 (2009).

[6]I. Kagomiya, J. Sugihara, K. Kakimoto, and H. Ohsato, "Mg_2SiO_4-TiO_2 Composite Ceramics Prepared Using a Liquid Phase Deposition Process," *J. Electroceram.*, **22** [1–3] 327–33 (2009).

[7]G. Dou, D. Zhou, M. Guo, S. Gong, and Y. Hu, "Low-Temperature Sintered Mg_2SiO_4-$CaTiO_3$ Ceramics with Near-Zero Temperature Coefficient of Resonant Frequency," *J. Mater. Sci.: Mater. Electron.*, **24** [5] 1431–8 (2013).

[8]T. S. Sasikala, C. Pavithran, and M. T. Sebastian, "Effect of Lithium Magnesium Zinc Borosilicate Glass Addition on Densification Temperature and Dielectric Properties of Mg_2SiO_4 Ceramics," *J. Mater. Sci.: Mater. Electron.*, **21** [2] 141–4 (2010).

[9]S. Meng, Z. Yue, H. Zhuang, F. Zhao, and L. Li, "Microwave Dielectric Properties of $Ba_3(VO_4)_2$-Mg_2SiO_4 Composite Ceramics," *J. Am. Ceram. Soc.*, **93** [2] 359–61 (2010).

[10]J. J. Zhang, J. W. Zhai, H. T. Jiang, and X. Yao, "Dielectric Tunable Properties of $Ba_{0.4}Sr_{0.6}TiO_3$-Mg_2SiO_4 Microwave Composite Ceramics," *Ferroelectrics*, **388** [1] 74–9 (2009).

[11]L. M. Wang, W. L. Gong, S. X. Wang, and R. C. Ewing, "Comparison of Ion-Beam Irradiation Effects in X_2YO_4 Compounds," *J. Am. Ceram. Soc.*, **82** [12] 3321–9 (1992).

[12]F. Tavangarian and R. Emadi, "Synthesis of Pure Nanocrystalline Magnesium Silicate Powder," *Ceram.-Silik.*, **54** [2] 122–7 (2010).

[13]K. X. Song, X. M. Chen, and X. C. Fan, "Effects of Mg/Si Ratio on Microwave Dielectric Characteristics of Forsterite Ceramics," *J. Am. Ceram. Soc.*, **90** [6] 1808–11 (2007).

[14]H. Naghib-Zadeh, C. Glitzky, W. Oesterle, and T. Rabe, "Low Temperature Sintering of Barium Titanate Based Ceramics with High Dielectric Constant for LTCC Applications," *J. Eur. Ceram. Soc.*, **31** [4] 589–96 (2011).

[15]D. X. Zhou, G. Dou, M. Guo, and S. P. Gong, "Low Temperature Sintering and Microwave Dielectric Properties of $ZnTiNb_2O_8$ Ceramics with BaCu(B_2O_5) Additions," *Mater. Chem. Phys.*, **130** [3] 903–8 (2011).

[16]D. Pamu, G. Lakshmi Narayana Rao, and K. C. James Raju, "Low Temperature Processing of $(Zr_{0.8}Sn_{0.2})TiO_4$ Ceramics with Improved Q Factor," *J. Alloys Compounds*, **509** [38] 9289–95 (2011).

[17]Y. P. Guo, H. Ohsato, and K. I. Kakimoto, "Characterization and Dielectric Behavior of Willemite and TiO_2-Doped Willemite Ceramics at Millimeter-Wave Frequency," *J. Eur. Ceram. Soc.*, **26** [10–11] 1827–30 (2006).

[18]F. Hanic, M. Handlović, K. Burdova, and J. Majling, "Crystal Structure of Lithium Magnesium Phosphate, $LiMgPO_4$: Crystal Chemistry of the Olivine-Type Compounds," *J. Crystallogr. Spectrosc. Res.*, **12** [2] 99–127 (1982).

[19]D. Thomas and M. T. Sebastian, "Temperature-Compensated $LiMgPO_4$: A New Glass-Free Low-Temperature Cofired Ceramic," *J. Am. Ceram. Soc.*, **93** [11] 3828–31 (2010).

[20]S. Ye, D. C. Yu, X. M. Wang, E. H. Song, and Q. Y. Zhang, "Anomalous Upconversion Emission of Eu^{3+}-Yb^{3+}-MoO_6 in Double Perovskites Induced by a Laser," *J. Mater. Chem. C*, **1** [8] 1588–94 (2013).

[21]O. Dernovsek, M. Eberstein, and W. A. Schiller, "LTCC Glass-Ceramic Composites for Microwave Application," *J. Eur. Ceram. Soc.*, **21** [10] 1693–7 (2001).

[22]R. D. Shannon, "Revised Effective Ionic Radii and Systematic Studies of Interatomic Distances in Halides and Chalcogenides," *Acta Crystallogr. Sec. A: Crys. Phys., Diffraction, Theoretical General Crystallogr.*, **32** [5] 751–67 (1976).

[23]L. M. Wang, W. L. Gong, S. X. Wang, and R. C. Ewing, "Comparison of Ion-Beam Irradiation Effects in X_2YO_4 Compounds," *J. Am. Ceram. Soc.*, **82** [12] 3321–9 (1999).

[24]A. Kirfel, T. Lippmann, P. Blaha, K. Schwarz, D. F. Cox, et al., "Electron Density Distribution and Bond Critical Point Properties for Forsterite, Mg_2SiO_4, Determined with Synchrotron Single Crystal X-ray Diffraction Data," *Phys. Chem. Miner.*, **32** [4] 301–13 (2005). □